Available online at www.sciencedirect.com
SCIENCE DIRECT®
Physica A 339 (2004) 152–158
PHYSICA A
www.elsevier.com/locate/physa

X-ray tomography for mesoscale physics applications

A. Sakellariou[a,*], T.J. Sawkins[a], T.J. Senden[a], A. Limaye[b]

[a] *Department of Applied Mathematics, Research School of Physical Sciences and Engineering, Australian National University, Canberra ACT 0200, Australia*
[b] *VizLab, Supercomputing Facility, Australian National University, Canberra ACT 0200, Australia*

Abstract

The field of mesoscale physics is concerned with length scales which lie in the sub-micron to millimetre range. As a subject, it covers complexity, disorder, cooperative effects and structure-property relationships. Much of modern material science can be found in this regime and it remains a rich ground for new research. As many of the phenomena ascribed to this regime span several orders in length scale and are inherently three-dimensional in nature, X-ray-computed tomography is a valuable tool in this field. A fully integrated facility dedicated to the study of mesoscopic phenomena is briefly described.

PACS: 07.85.−m; 81.70.Tx; 87.59.Fm

Keywords: Computed tomography; Mesoscale physics

1. Introduction

For many years, this department has been active in the fields of intermolecular forces, surface chemistry, surface physics and molecular self-assembly at the nano-scale. The properties at this scale play an important part in understanding the physical and transport properties of materials at larger scales, especially the affects of topology and surface form. This work has recently been extended to the mesoscale. At this scale, the traditional domains of physics, chemistry, biology and geology merge. To experimentally investigate this scale, a purpose built X-ray tomography facility was commissioned to investigate all media, be it porous, disordered or complex.

* Corresponding author. Tel.: +61-2-61254975; fax: +61-2-61250732.
E-mail address: arthur.sakellariou@anu.edu.au (A. Sakellariou).

0378-4371/$ - see front matter
doi:10.1016/j.physa.2004.03.055

Based on X-rays, the instrument is designed to have a large field of view (2048^3 voxels and 60 mm cross-section), high spatial resolution (2 μm), high dynamic range for enhanced contrast (16 bits), sufficient throughput to permit slow time series experiments and with ample versatility to implement and develop various contrast enhancing imaging techniques. The facility has collected, processed and analysed, both as static and in some cases as composite dynamic data sets, 240 tomograms with 1024^3 voxels and 20 tomograms with 2048^3 voxels in 1 year. This includes sedimentary rocks, soils, bone, soft tissue, ceramics, fibre-reinforced composites, foams, wood, paper and small animals.

2. X-Ray tomography

Tomography is a technique that generates a data set, called a *tomogram*, which is a three-dimensional representation of the structure and variation of composition within a specimen. Each three-dimensional point in the tomogram is called a *voxel*. At this facility, X-rays from a micro-focus X-ray source are used to probe the specimen and an X-ray camera is used to record the X-ray transmission radiograph. To generate the tomogram, a series of radiographs are collected at different viewing angles by rotating the specimen. This set of radiographs, called *projection* data, are processed with a reconstruction algorithm to generate the tomogram of the specimen.

2.1. The instrument

The instrument, shown in Fig. 1, is built on a 3 m parallel optical rail. The X-ray source is fixed at one end and both the rotation and detector stages are mounted on linear bearings. By translating these stages, magnifications can be set between 1.1× to over 100×, thus utilising either the large field (60 mm cross-section with 30 μm voxel size) or high-resolution (4 mm cross-section with 2 μm voxel size) aspect of

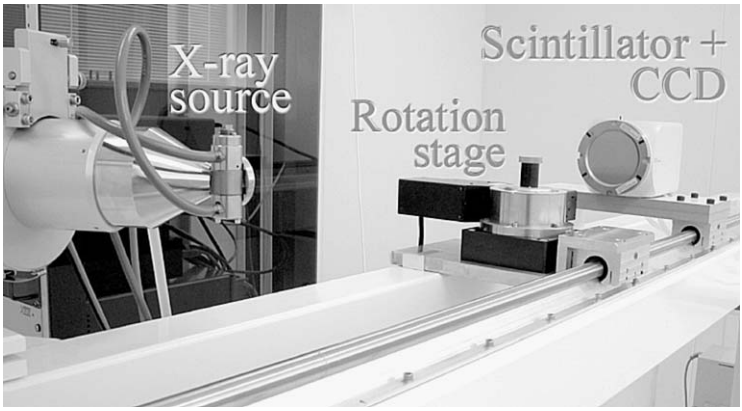

Fig. 1. A photo of the X-ray tomography instrument.

Table 1
Characteristics of the X-ray Tomography experiments at this facility

Voxels	Projections	Data size	Acquisition times (h)
512^3	800	400 MB	$\frac{3}{4}$–10
1024^3	1600	3.1 GB	3–28
2048^3	3000	24 GB	15–48

the instrument. To explore various contrast enhancing techniques, sufficient clearance about the rotation stage is available to attach various experimental apparatus.

The X-ray Source (X-Tek RTR-UF225) uses a focused electron beam to generate a polychromatic X-ray beam via bremsstrahlung (30–225 kV/1 mA with 2–5 μm spot size). The X-ray Shutter (built in-house) blanks the X-ray beam with a 2.5 mm thick piece of platinum. The Rotation Stage (Newport RV120PP) rotates the specimen during data collection, with an accuracy of 1 milli-degree. It has high rigidity and is capable of supporting axial loads of up to 100 kg. The X-ray Camera (Roper PI-SCX100:2048) records the X-ray radiographs. It has an active area of 70×70 mm^2 with 2048×2048 16-bit pixels and a download time of 1 Megapixel per second.

2.2. The experiment

The X-ray source produces a polychromatic X-ray beam and the projection data are collected with a cone beam along a circular trajectory. Even though such characteristics are less than ideal for tomography, high quality and accurate tomograms are generated with this instrument. Polychromatic X-rays result in the phenomenon of beam hardening, which introduces artifacts into the tomogram. To minimise this, the X-ray beam is pre-filtered. Typically, the filter is chosen to have a similar composition to the specimen and with a thickness about 37% (e^{-1}) the diameter of the specimen. Cone beam geometry can only generate accurate tomograms if Tuy's sufficiency condition [1] is satisfied. With a circular geometry, problems predominate if specimens consist of a periodic distribution of parallel planar edges, in which their normals are aligned parallel to the rotation axis. With mesoscale physics applications, specimens typically do not have such structure. Nevertheless, to minimise any problems, a small cone beam angle is utilised. The camera length is typically set to 2500 mm and since the active area of the X-ray camera is 70×70 mm^2, this results in a cone angle of only 0.8°.

Since the projection data are collected with a cone beam geometry, the specimen must be rotated through 360°. The optimal number of projections, N_θ, is given by $N_\theta = (\pi/2)N_w$, where N_w is the number of pixels in the width of the detector. This number ensures that there is adequate angular sampling to accurately reconstruct the specimen. In Table 1, various experimental characteristics are listed for the most common tomogram sizes. The total acquisition time of an experiment depends on many factors, the main being whether beam filtering is used. Even though this can lead to a significant increase in the duration of the experiment, the reduction in beam hardening artifacts more than compensates for the inconvenience.

Table 2
Resources required for pre-processing and reconstructing projection data

Voxels	Pre-processing			Reconstruction		
	CPUs	RAM	Time (min)	CPUs	RAM	Time (min)
512^3	2	1.6 GBytes	4	4	800 MBytes	9
1024^3	16	12 GBytes	8	32	7 GBytes	40
2048^3	128	108 GBytes	35	128	60 GBytes	211

2.3. The reconstruction

To generate a tomogram, the projection data must represent linear interactions between the specimen and the probe. For X-ray tomography, the interaction is non-linear and is dominated by X-ray attenuation. Ignoring subtle X-ray interaction phenomena, Beer's law of attenuation is an accurate description of the specimen–probe interaction. Beer's law is easy to manipulate into a linear form, provided the X-ray beam is mono-energetic. This linearisation also works for the poly-energetic case but beam hardening artifacts are introduced into the tomogram, which is why the X-ray beam is pre-filtered to minimise it's energy spread. Once the projection data are linearised, other steps follow to minimise artifacts in the tomogram that are the result of non-ideal aspects of the experiment. The most common are the result of cosmic rays, defects, non-linear sensitivity and spatial non-linearity in the X-ray camera, misaligned cone beam geometry and specimen rotation and variability of the X-ray flux from the source. A description of these problems and the algorithms implemented to reduce their effect is beyond the scope of this paper (see Ref. [2]).

Reconstruction relies on two processes, a pre-processing step followed by a Feldkamp reconstruction step [3]. Table 2 indicates the computational resources required for the three most common tomogram sizes. All data processing is performed at the Australian Partnership for Advanced Computing (APAC) national facility [4], which houses a Compaq AlphaServer super-computer. To date, over 2 Terabytes of data have been collected.

2.4. A Comparison to other facilities

A multitude of X-ray tomography modalities have been developed [5]. To analyse specimens typical in mesoscale physics research, a system based on X-ray attenuation is most appropriate.

The approach to use a cone beam geometry is not original [3]. Indeed, several modern facilities exist [6–8], including several companies that sell complete systems [9–11]. But there are three issues which typically set our facility apart from others: the detector, the path length and the sample space. Detectors are limited to an 8-, 12- or 14-bit dynamic range with around a million pixels. Path lengths are much less than a metre in length which implies larger cone angles. Finally, the sample space greatly restricts the inclusion of experimental equipment.

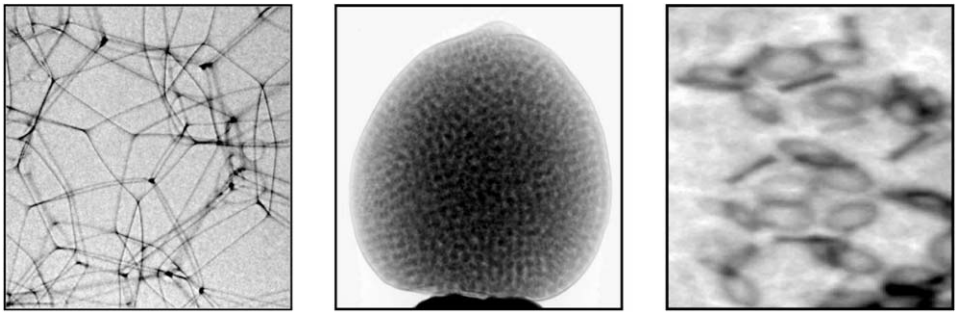

Fig. 2. Radiographic projections from the ANU CT Facility. (a) 1–2 mm soap bubbles, (b) 8000, 2 mm acrylic beads in a balloon, (c) X-ray opaque toroidal condensates form between contacting (transparent) 1.5 mm carbon beads.

The main problem with synchrotron facilities [6–8] is the difficulty to secure sufficient access, especially when studing dynamical systems with long equilibriation times. Nevertheless, two advantages remain; tunable mono-energetic X-rays and better resolution. Tunable energy allows elemental discrimination, something that is difficult to achieve with a conventional source. However, better resolution results in the loss of dynamic range and flux [12]. The beam of a synchrotron is at best weakly divergent, thus the detector pixels need to be physically small to maximise field of view. The penalty is the dynamic range is often restricted to only 8-bits.

3. Examples of data

Figs. 2 and 3 illustrate some of the systems studied at the facility. In most cases, the tomograms are segmented into binary images for analysis [13]. The types of analysis include: imaging multiphase flow in porous media [14], deriving foam properties [15], investigating the morphology of self-assembled colloids [16], analysing Haversian canals in bones [17], investigating geometrical structure in sphere packs [18] and deriving petrophysical properties [19].

Acknowledgements

The authors thank the Australian Research Council (ARC) for support of the hardware development and Australian Partnership for Advanced Computing for access. Additional support of hardware development, and Sakellariou's appointment was provided by Cooperative Research Centre for Functional Communication Surfaces. Senden gratefully acknowledges the ARC for his Fellowship.

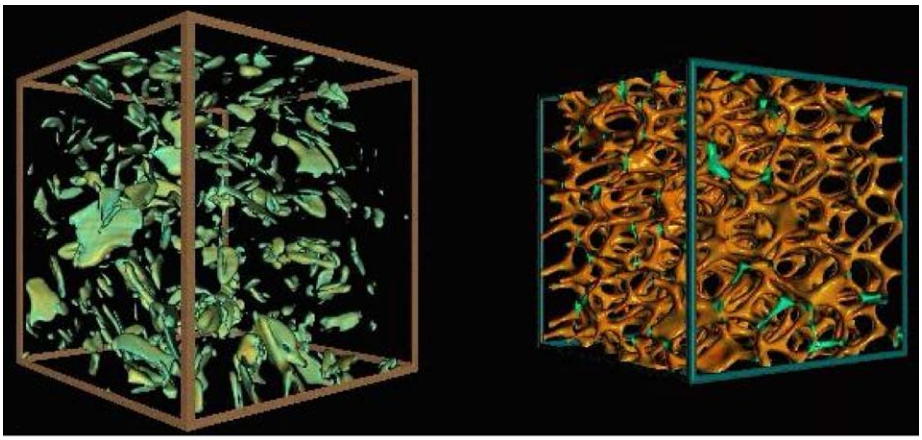

Fig. 3. Tomograms from the ANU CT Facility. Movies are available at the URL: http://www.rsphysse.anu.edu.au/appmaths/ct_movies. (a) 500 μm bounding box showing films of condensate within the contacts formed by an irregular, faceted grain pack. Grains have been made transparent. (b) 500 μm bounding box showing the plateau structures within an open cell aluminium foam (a replica of a polymer foam pre-form).

References

[1] H.K. Tuy, An inversion formula for cone-beam reconstruction, Siam J. Appl. Math. 43 (3) (1983) 546–552.
[2] A. Sakellariou, T.J. Sawkins, T.J. Senden, Internal ANU Document, in preparation.
[3] L.A. Feldkamp, L.C. Davis, J.W. Kress, Practical cone-beam algorithm, J. Opt. Soc. Am. A 1 (1984) 612–619.
[4] http://nf.apac.edu.au/facilities/sc/hardware.php.
[5] C.A. Carlsson, Imaging modalities in X-ray computerised tomography and in selected volume tomography, Phys. Med. Biol. 44 (1999) R23–56.
[6] U. Bonse (Ed.), Developments in X-ray tomography, Proc. SPIE 3149 (1997).
[7] U.Bonse (Ed.), Developments in X-ray tomography II, Proc. SPIE 3772 (1999).
[8] U.Bonse (Ed.), Developments in X-ray tomography III, Proc. SPIE 4503 (2002).
[9] http://www.skyscan.be/next/home.htm.
[10] http://www.scanco.ch.
[11] http://www.aeat.com/ndt/tomohawk/tomohawk.html.
[12] M.J. Flynn, S.M. Hames, S.J. Wilderman, D.A. Reimann, Comparison of X-ray sources for 3D microtomography, Nucl. Instrum. Methods A 353 (1994) 312–315.
[13] A.P. Sheppard, R.M. Sok, H. Averdunk, Techniques for image enhancement and segmentation of tomographic images of porous materials, Physica A (2004), these proceedings, doi:10.1016/j.physa.2004.03.057.
[14] M. Turner, L. Knüfing, C.H. Arns, A. Sakellariou, T. Senden, A.P. Sheppard, R.M. Sok, A. Limaye, W.V. Pinczewski, M.A. Knackstedt, Three dimensional imaging of multiphase flow in porous media, Physica A (2004), these proceedings, doi:10.1016/j.physa.2004.03.059.
[15] M. Saadatfar, M.A. Knackstedt, C.H. Arns, A. Sakellariou, T. Senden, A.P. Sheppard, R.M. Sok, H. Steininger, W. Schrof, Polymeric foam properties derived from 3D images, Physica A (2004), these proceedings, doi:10.1016/j.physa.2004.03.054.

[16] S.T. Hyde, A.M. Carnerup, A.-K. Larsson, A.G. Christy, J.M. Garcia-Ruiz, Self-assembly of carbonate-silica colloids: between living and non-living form, Physica A (2004), these proceedings, doi:10.1016/j.physa.2004.03.045.

[17] A.C. Jones, A.P. Sheppard, R.M. Sok, C.H. Arns, A. Limaye, H. Averdunk, A. Brandwood, A. Sakellariou, T.J. Senden, B.K. Milthorpe, M.A. Knackstedt, Three-dimensional analysis of cortical bone structure using X-ray micro-computed tomography, Physica A (2004), these proceedings, doi:10.1016/j.physa.2004.03.046.

[18] T. Aste, M. Saadatfar, A. Sakellariou, T.J. Senden, Investigating the geometrical structure of disordered sphere packings, Physica A (2004), these proceedings, doi:10.1016/j.physa.2004.03.034.

[19] C.H. Arns, A. Sakellariou, T.J. Senden, A.P. Sheppard, R.M. Sok, W.V. Pinczewski, M.A. Knackstedt, Petrophysical properties derived from X-ray CT images, APPEA J. (2003) 577–586.